

## Non-Isothermal Crystallization Kinetics of Graphene Oxide-Carbon Nanotubes Hybrids / Polyamide 6 Composites

<sup>1,2</sup> Zhi-Qiang Wang, <sup>2,3</sup> Yong-Ke Zhao and <sup>2</sup>Xiang-Feng Wu\*

<sup>1</sup> College of Materials Science and Engineering, North University of China, Taiyuan 030051, China.

<sup>2</sup> School of Materials Science and Engineering, Hebei Provincial Key Laboratory of Traffic Engineering Materials, Shijiazhuang Tiedao University, Shijiazhuang 050043, China.

<sup>3</sup> College of Materials Science and Engineering, State Key Laboratory of Chemical Resource Engineering, Beijing University of Chemical Technology, Beijing 100029, China.

Zhi-Qiang Wang and Yong-Ke Zhao contributed equally to this work and share the first authorship.

wuxiangfeng@stdu.edu.cn\*

(Received on 29<sup>th</sup> November 2017, accepted in revised from 10<sup>th</sup> November 2018)

**Summary:** The hybrids combined by nano-materials with different dimensions usually possess much better enhancement effects than single one. Graphene oxide-carbon nanotubes hybrids / polyamide 6 composites has been fabricated. The non-isothermal crystallization kinetics of the as-prepared samples was discussed. Research results showed that increasing the cooling rate was in favor of increasing the crystallization rate and the degree of crystallinity for the as-prepared samples. Moreover, the crystallization rate was first decreased and then increased with increasing the hybrids loading. Furthermore, the crystallization mechanism was changed with increasing the crystallization temperature and the cooling rate. The nucleation and growth modes of the non-isothermal crystallization could be classified into three different types, according to the Ozawa's theory. These complicated results could be attributed to the important role of crystallization rate as well as the simultaneous hindering and promoting effects of the as-prepared hybrids. This work has reference values for understanding the crystallization kinetics of the polyamide 6-based composites.

**Keywords:** Polyamide 6; Carbon nanotubes; Graphene oxide; Non-isothermal crystallization; Crystallization activation energy.

### Introduction

Polyamide 6 (PA6) is a kind of important thermoplastic polymers with excellent mechanical properties, solvent resistance and good processability [1-4]. However, PA6 displays some inherent weaknesses, such as poor dimension stability, low heat distortion temperature and high moisture sorption (2.5%), which are detrimental for its practical applications [5]. These properties of PA6 depend on the degree of crystallinity and crystal morphology, which is controlled by the crystallization conditions. Therefore, regulating crystallization process is a key point to improve the performances of the final products.

Generally, nano-sized fillers usually have obvious effects on the crystallization behaviors of semi-crystalline polymers. These fillers include boron nitride, silicon dioxide, clay, glass fiber, montmorillonite, carbon nanotubes (CNTs), graphene and graphene oxide (GO) [6-14]. Besides, the hybrids combined by nano-materials with different dimensions have attracted much more attention due to their collaborative advantages [15-17]. One of the typical examples is that the hybrids of GO/CNTs

possess much better enhancement effects than single filler [18, 19]. The GO/CNTs hybrids have been introduced into many kinds of polymers, such as epoxy, polyvinyl alcohol, polyaniline and polystyrene [20-25]. However, to our knowledge, no related works have been reported about the crystallization properties of the GO-CNTs / PA6 composites. Moreover, due to the complex influence factors, it is still a challenging for explicitly understanding the crystallization kinetics of the semi-crystalline polymer composites.

Herein, the GO-CNTs hybrids has been prepared and blended with PA6 to fabricate the composite films. The non-isothermal crystallization behaviors of the as-prepared composites have been discussed by using Jeziorny, Ozawa, Mo and Kissinger's theories, respectively. The results could provide reference values for studying the crystallization behaviors of the PA6-based composites.

---

\*To whom all correspondence should be addressed.

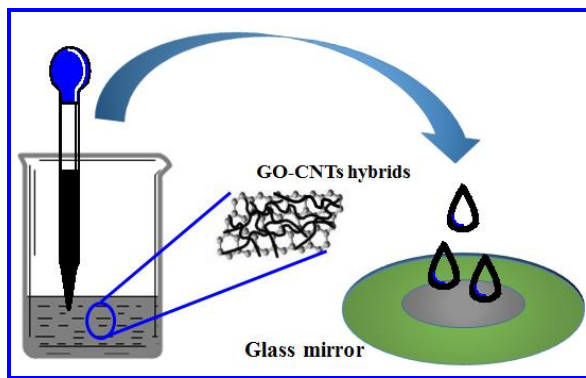
## Experimental

### Materials

The GO-CNTs hybrids have been prepared in our laboratory [26]. PA6 were bought from Shanghai Kingfa Technology Development Co., Ltd., China. Formic acid (HCOOH) has been bought from Tianjin Hongyan Reagent Factory, China.

### Preparation of the GO-CNTs / PA6 composites

PA6 (5 g) was mixed with HCOOH (50 mL) at 60 °C for 1 h. Then, the as-prepared GO-CNTs hybrids were added into the above solution. Subsequently, the PA6-based films with various contents of the as-obtained hybrids (0, 0.3, 0.6 or 0.9 wt%) were prepared by using a solution casting method (Scheme-1). Finally, the as-prepared films were dried in an electric vacuum drying oven at 60 °C for 12 h. The as-prepared products were named as PA6, PA6-0.3, PA6-0.6 or PA6-0.9 according to the GO-CNTs hybrids loading, respectively.



Scheme-1: Schematic diagram of preparation process of the GO-CNTs / PA6 composites.

### Characterization

Non-isothermal crystallization behaviors of the as-prepared GO-CNTs / PA6 composite films has been characterized by using differential scanning calorimetry (DSC, Model: METTLER TOLEDO DSC822<sup>e</sup>, Switzerland) under the protection of argon atmosphere. A typical process is shown as follows: the as-prepared films were firstly heated to 250 °C (at 50 °C·min<sup>-1</sup>) and maintained for 3 min to eliminate residual crystals. Subsequently, the melt was cooled to 25 °C at various cooling rates (5, 10, 20 or 40 °C·min<sup>-1</sup>). The cooling process were recorded and analyzed.

## Results and Discussion

### Thermograms

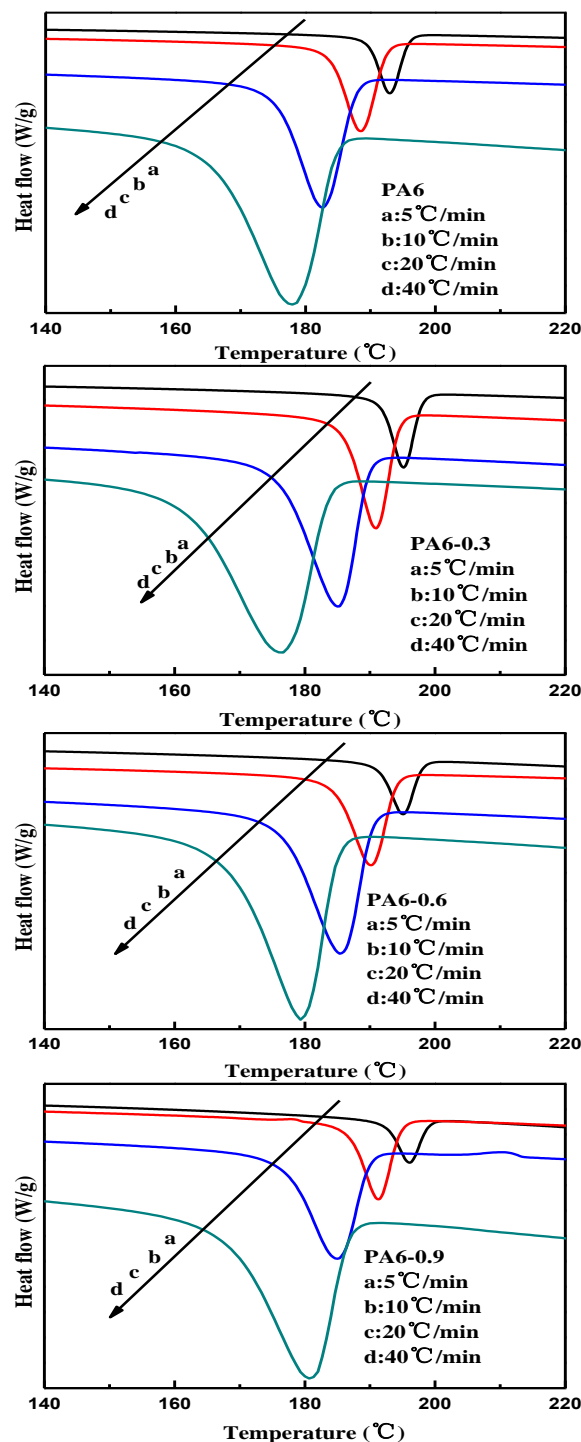


Fig. 1: Heat flow versus Temperature ( $T$ ) of the samples at various cooling rates ( $\phi$ ).

The non-isothermal crystallization curves of the as-obtained GO-CNTs / PA6 composites are shown in Fig.1. It can be observed that the peak temperature ( $T_p$ ) was gradually moved to low temperature region with increasing  $\phi$ . This phenomenon was caused by that the molecular chains of the PA6 matrix would be arranged during the cooling process. Moreover, if the  $\phi$  was too fast, the molecular chains would not be completely arranged and cause the  $T_p$  to be low.

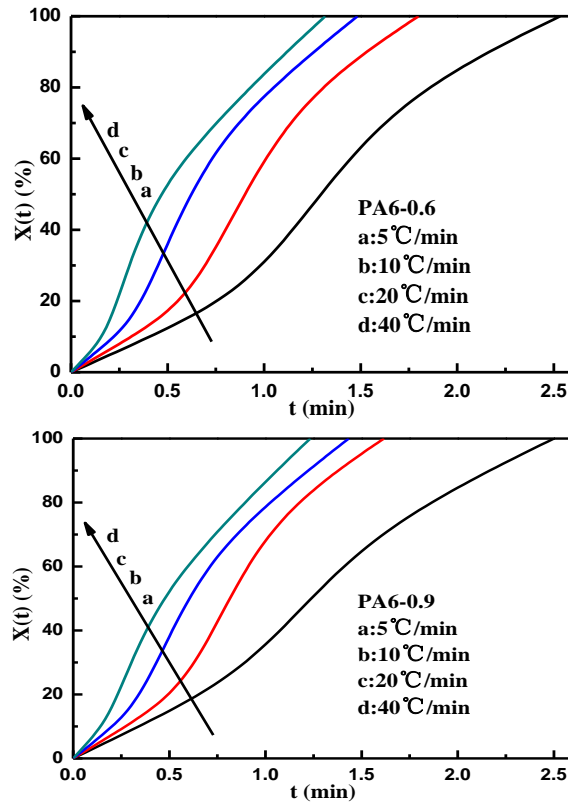
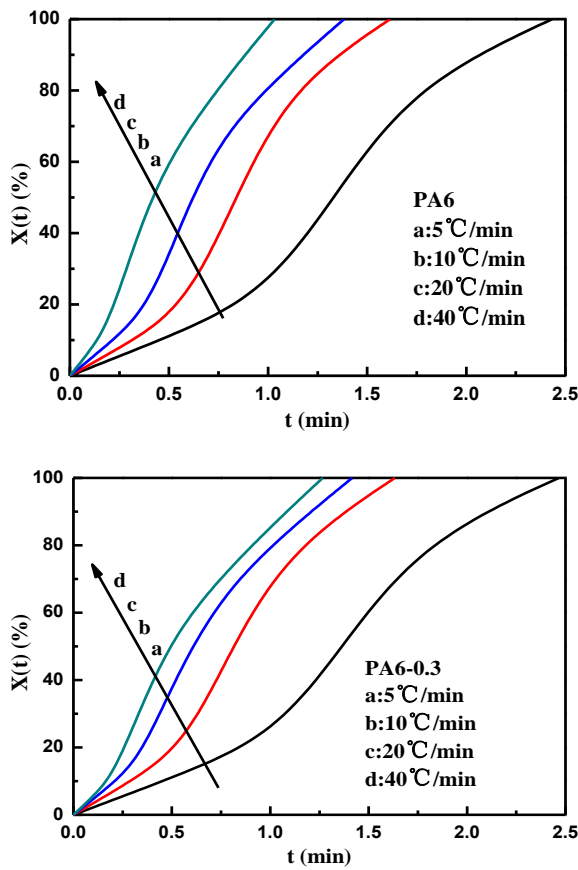


Fig. 2: Relative crystallinity  $X(t)$  versus Time ( $t$ ) of the samples at various  $\phi$ .

Fig. 2 shows the curves of relative crystallinity  $X(t)$  versus Time ( $t$ ). Moreover, Table-1 shows the halftime of crystallization ( $t_{1/2}$ ) and overall crystallization rate ( $G$ , which could be usually calculated by using the Equation (1)).

$$G = \frac{1}{t_{1/2}} \quad (1)$$

Table-1:  $G$  of the samples at various  $\phi$ .

$\phi$	PA6	PA6-0.3	PA6-0.6	PA6-0.9
$5^{\circ}\text{C}\cdot\text{min}^{-1}$	$t_{1/2}$ (min)	1.33	1.37	1.30
	$G$ (min $^{-1}$ )	0.75	0.73	0.77
$10^{\circ}\text{C}\cdot\text{min}^{-1}$	$t_{1/2}$ (min)	0.85	0.82	0.92
	$G$ (min $^{-1}$ )	1.18	1.22	1.09
$20^{\circ}\text{C}\cdot\text{min}^{-1}$	$t_{1/2}$ (min)	0.63	0.62	0.63
	$G$ (min $^{-1}$ )	1.59	1.61	1.59
$40^{\circ}\text{C}\cdot\text{min}^{-1}$	$t_{1/2}$ (min)	0.43	0.50	0.48
	$G$ (min $^{-1}$ )	2.33	2.00	2.08

From Fig. 2 and Table-1, it can be found that the time range became narrower and narrower with increasing  $\phi$ . Furthermore, Fig. 2 and Table 1 revealed that: (1) the  $G$  of the as-prepared GO-CNTs / PA6 composites was increased with increasing  $\phi$ ; (2) there was a proper  $\phi$  for the as-prepared composites. If  $\phi$  was too slow (such as  $5 \text{ }^{\circ}\text{C} \cdot \text{min}^{-1}$ ) or too fast (such as  $40 \text{ }^{\circ}\text{C} \cdot \text{min}^{-1}$ ), the  $G$  of the as-prepared composites would increase with increasing the fillers loading. These results could be explained by that the GO-CNTs hybrids could restrict the motion of chain segments, which obviously influenced  $G$ . Moreover, the GO-CNTs hybrids could play as nucleating agents to increase the  $G$  of the composites. Therefore, the two coexisting reasons resulted in various  $G$ .

#### Avrami theory modified by Jeziorny

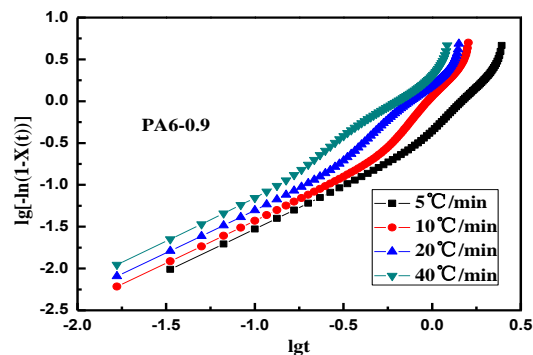
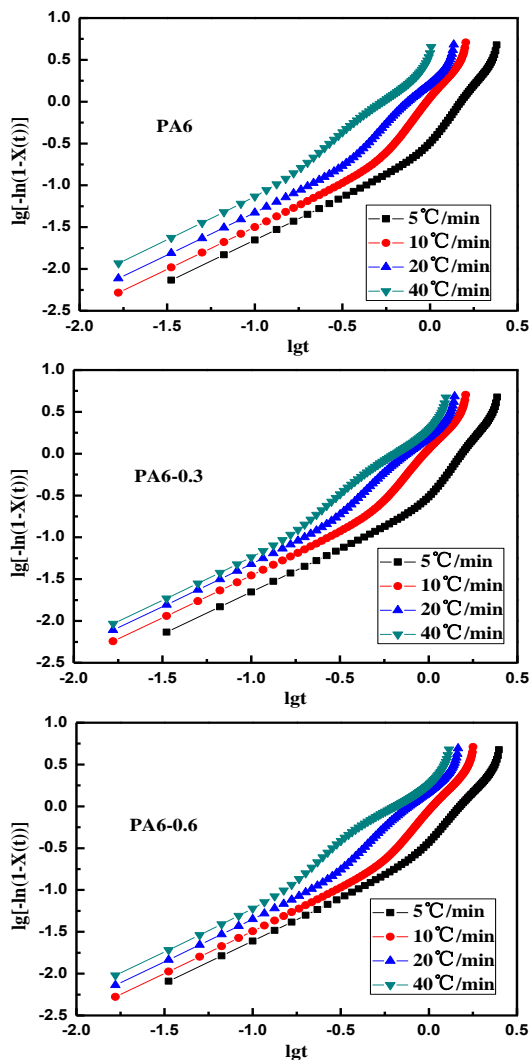


Fig. 3:  $\lg[-\ln(1-X(t))]$  versus  $\lg t$  of the samples at various  $\phi$ .

Generally, the initial stage of non-isothermal crystallization can be analyzed by using the flowing Equations (2) and (3):

$$1 - X(t) = \exp(-Z_t t^n) \quad (2)$$

$$\lg[-\ln(1 - X(t))] = n \lg t + \lg Z_t \quad (3)$$

where  $X(t)$ ,  $n$  and  $Z_t$  is the relative crystallinity, the nucleation and the growth exponent as well as the growth rate constant, respectively. Generally, the larger the  $Z_t$ , the higher the  $G$  is. However, considering the non-isothermal character, Jeziorny suggested  $Z_t$  should be corrected by the following Equation (4) [27]:

$$\lg Z_c = \frac{\lg Z_t}{\phi} \quad (4)$$

According to above Equations, the curves of  $\lg[-\ln(1-X(t))]$  versus  $\lg t$  and the data could be obtained. They are shown in Fig. 3 and Table-2, respectively.

It can be seen in Fig. 3 and Table 2 that: (1) the  $n$  of the as-prepared GO-CNTs / PA6 composites was first increased and then decreased with increasing  $\phi$ . Moreover, it was gradually decreased with increasing the fillers loading; (2) the  $Z_c$  was gradually increased with increasing  $\phi$  for pure PA6, while first increased and then decreased for the composite samples; (3) for a fixed  $\phi$  (such as  $20 \text{ }^{\circ}\text{C} \cdot \text{min}^{-1}$ ), the  $Z_c$  was almost unchanged with increasing the fillers loading. These results manifested that increasing  $\phi$  was in favor of increasing  $G$ , and has obvious effects on the nucleation and the growth mechanism.

Table-2:  $\lg Z_t$ ,  $n$ ,  $\lg Z_c$  and  $Z_c$  of the samples at various  $\phi$ .

$\phi$		PA6	PA6-0.3	PA6-0.6	PA6-0.9
$5^{\circ}\text{C}\cdot\text{min}^{-1}$	$\lg Z_t$	-0.29	-0.31	-0.27	-0.23
	$n$	1.61	1.59	1.55	1.47
	$\lg Z_c$	-0.058	-0.062	-0.054	-0.046
	$Z_c$	0.875	0.867	0.883	0.899
$10^{\circ}\text{C}\cdot\text{min}^{-1}$	$\lg Z_t$	0.02	0.03	-0.04	0.03
	$n$	1.64	1.60	1.58	1.57
	$\lg Z_c$	0.002	0.003	-0.004	0.003
	$Z_c$	1.005	1.007	0.991	1.007
$20^{\circ}\text{C}\cdot\text{min}^{-1}$	$\lg Z_t$	0.19	0.19	0.17	0.19
	$n$	1.56	1.53	1.54	1.51
	$\lg Z_c$	0.0095	0.0095	0.0085	0.0095
	$Z_c$	1.022	1.022	1.020	1.022
$40^{\circ}\text{C}\cdot\text{min}^{-1}$	$\lg Z_t$	0.41	0.29	0.29	0.30
	$n$	1.49	1.48	1.44	1.41
	$\lg Z_c$	0.01025	0.00725	0.00725	0.00750
	$Z_c$	1.024	1.017	1.017	1.017

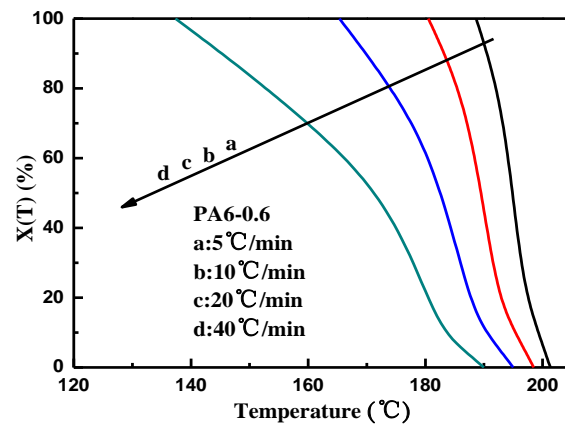
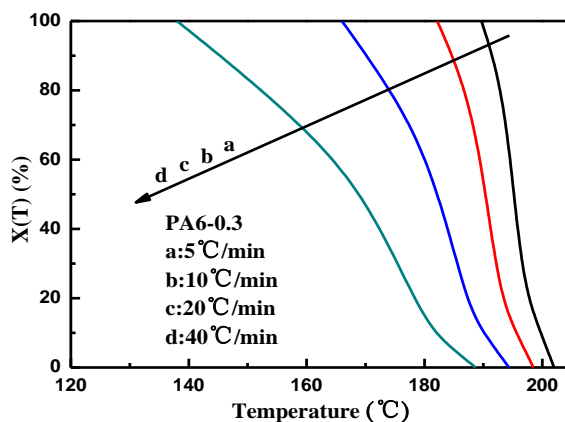
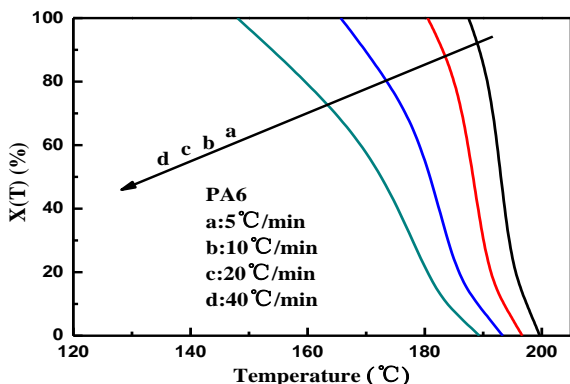
*Avrami theory modified by Ozawa*

According to Ozawa's theory,  $X(T)$  can be analyzed by the Equations (5) and (6) [28]:

$$\ln(1-X(T)) = -K(T)\phi^m \quad (5)$$

$$\lg[-\ln(1-X(T))] = \lg K(T) - m \lg \phi \quad (6)$$

where  $m$  and  $K(T)$  is the Ozawa exponent and the cooling crystallization function related to the overall  $G$ , respectively. According to Equations (5) and (6), the curves of the relative crystallinity  $X(T)$  versus Temperature ( $T$ ) could be acquired, as is shown in Fig. 4



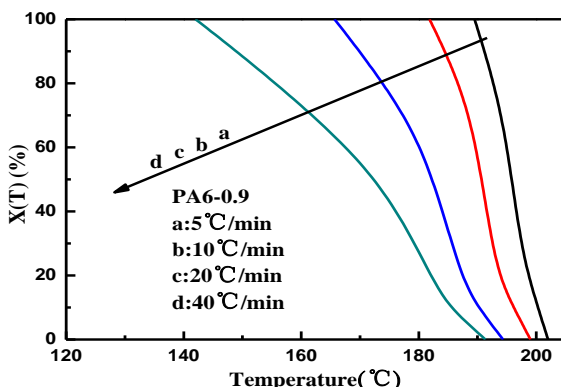


Fig. 4: Relative crystallinity  $X(T)$  versus Temperature ( $T$ ) of the samples at various  $\phi$ .

It can be observed that all of the curves showed reverse 'S' patterns. This phenomenon revealed that only the effects of  $\phi$  on the crystallization could be found.

Fig. 5 shows  $\lg[-\ln(1-X(T))]$  versus  $\lg \phi$  of the samples at various  $\phi$ . It manifested that the poor linearity made it difficult to obtain credible results. Because the non-isothermal crystallization process was dynamic, the  $G$  was not a constant but a function with regard to  $T$  and  $\phi$ . These curves could be divided into three parts depending on  $\phi$ . The  $m$  and  $\lg K(T)$  can be obtained by the slope and intercept of the curves. The plots of  $\lg K(T)$  and  $m$  versus  $T$  at various  $\phi$  were showed in Fig. 6.

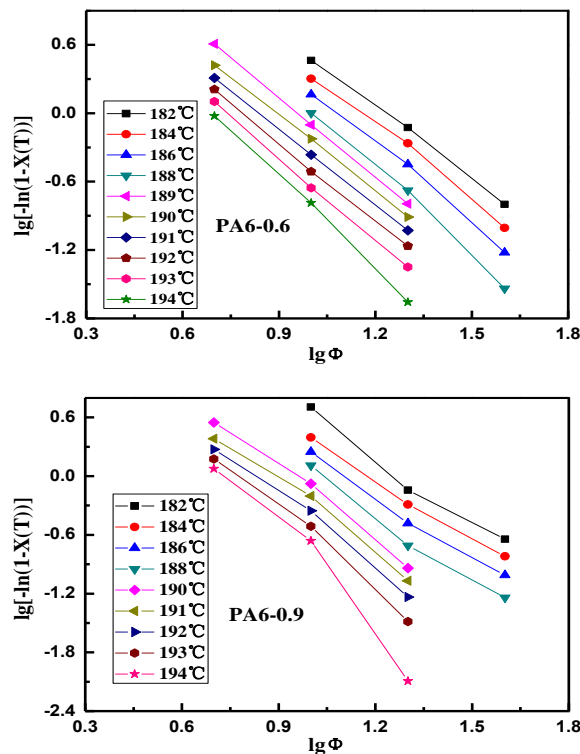
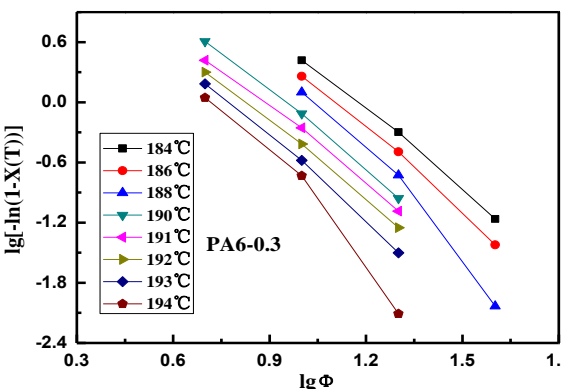


Fig. 5:  $\lg[-\ln(1-X(T))]$  versus  $\lg \phi$  of the samples at various  $\phi$ .

It can be seen in Fig. 6 that both the  $\lg K(T)$  and  $m$  of the as-prepared samples were firstly decreased, secondly increased, thirdly decreased and finally increased with increasing the crystallization temperature. According to this phenomenon, it could be concluded that the crystallization mechanism has been changed with crystallization temperature and  $\phi$ . Moreover, the nucleation and growth mode could be classified into three different types : (1) it was first three-dimensional (3D) and then 2D for all the as-prepared samples at 5-10  $^{\circ}\text{C}\cdot\text{min}^{-1}$ ; (2) it was first 3D and then 2D for pure PA6, PA6-0.3 and PA6-0.9 at 10-20  $^{\circ}\text{C}\cdot\text{min}^{-1}$ ; (3) it was 2D for PA6, PA6-0.6 and PA6-0.9 at 20-40  $^{\circ}\text{C}\cdot\text{min}^{-1}$ .

#### Mo's equation

Mo et al. has adopted the Equation (7) to discuss the non-isothermal crystallization process [29]:

$$\lg \phi = \lg F(T) - \alpha \lg t \quad (7)$$

where  $\alpha$  is the ratio of the Avrami and Ozawa exponent.

The values of  $\alpha$  and  $\lg F(T)$  could be usually obtained from the slope and intercept of the curves. The results are showed in Fig. 7 and Table-3.

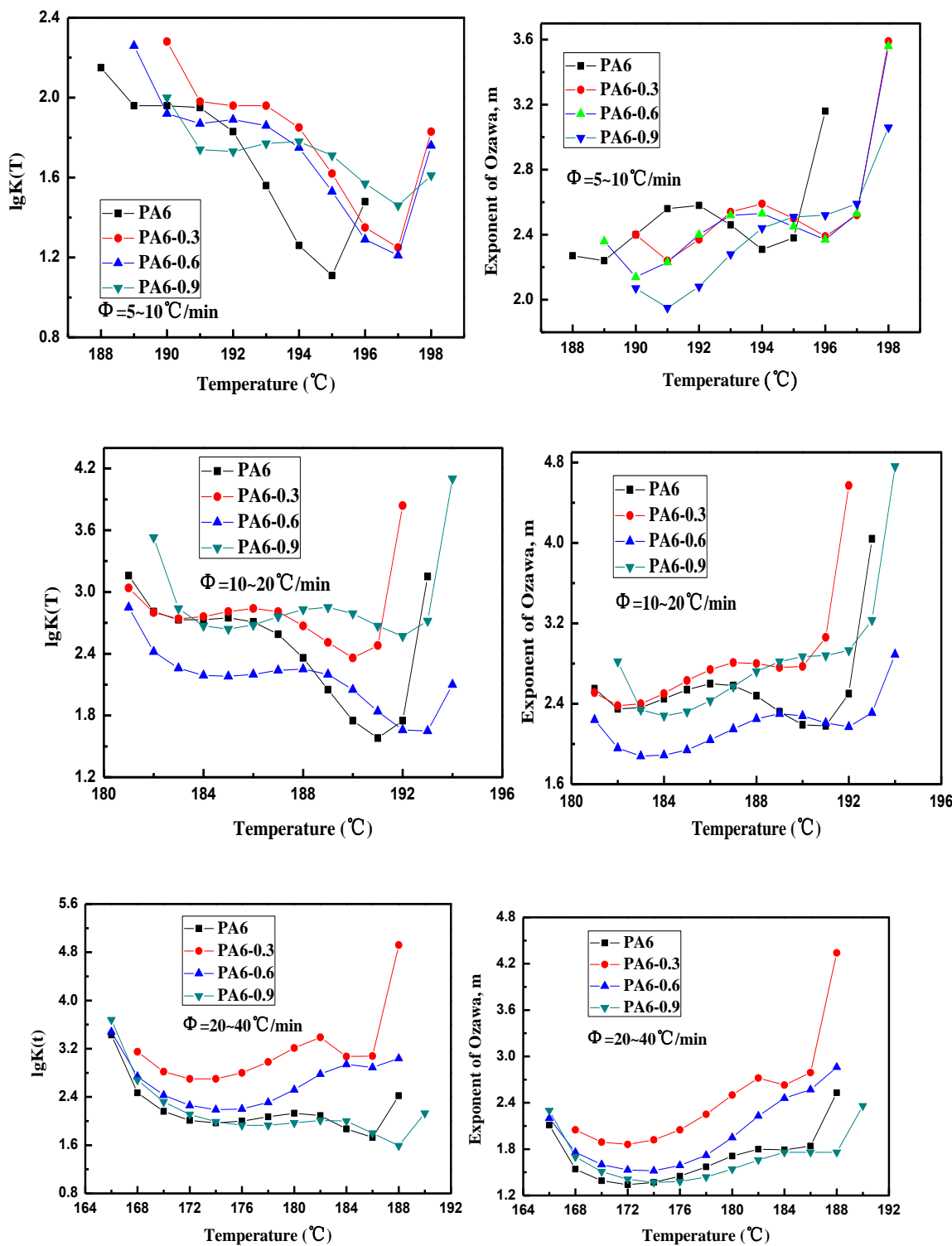
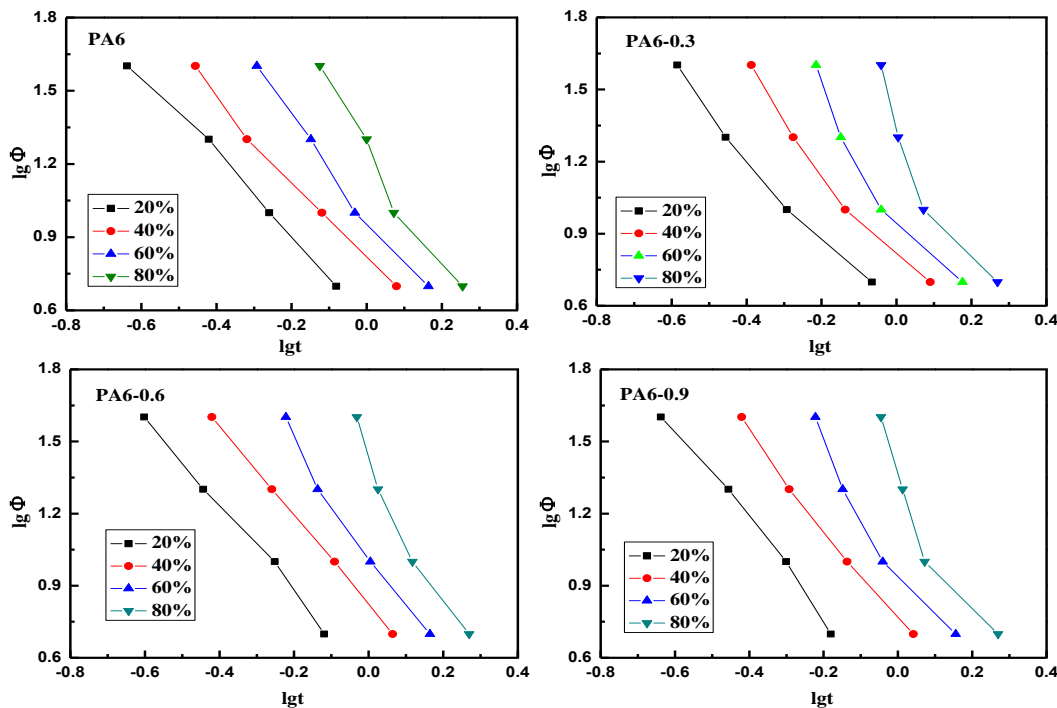


Fig. 6:  $\lg K(T)$  and  $m$  versus Temperature ( $T$ ) of the samples at various  $\phi$

Fig. 7:  $\lg \phi$  versus  $\lg t$  of the samples.Table-3:  $\alpha$  and  $\lg F(T)$  of the samples.

	$X(t)\text{ (%)}$	PA6	PA6-0.3	PA6-0.6	PA6-0.9
20	$\alpha$	1.636	1.720	1.827	1.954
	$\lg F(T)$	0.578	0.549	0.503	0.381
40	$\alpha$	1.656	1.864	1.855	1.944
	$\lg F(T)$	0.813	0.820	0.823	0.758
60	$\alpha$	2.001	2.193	2.277	2.310
	$\lg F(T)$	0.996	1.025	1.042	1.003
80	$\alpha$	2.410	2.672	2.891	2.688
	$\lg F(T)$	1.272	1.354	1.426	1.358

It can be observed in Fig. 7 and Table-3 that: (1) the  $\lg F(T)$  was gradually increased with increasing  $X(t)$ ; (2) when  $X(t)$  was equal or greater than 40 %, the  $\lg F(T)$  was first increased and then decreased with increasing the GO-CNTs hybrids loading. When the hybrids loading was 0.6 wt%, the  $\lg F(T)$  was reached the maximum. It showed that the  $G$  of the as-prepared sample was the smallest. These results were attributed to that high  $\phi$  was in favor of achieving high  $X(t)$ . Moreover, the as-prepared GO-CNTs hybrids could act as physical obstacles to decrease the  $G$  or heterogeneous nucleation agents to increase the  $G$ .

These two reasons resulted in various  $G$ .

#### Crystallization activation energy

Considering the influences of the  $\phi$ , the activation energy ( $\Delta E$ ) can be analyzed by the Equation (8) [30]:

$$\frac{d \left[ \ln \left( \frac{\phi}{T_p^2} \right) \right]}{d \left( \frac{1}{T_p} \right)} = -\frac{\Delta E}{R} \quad (8)$$

where  $R$  is the gas constant.

According to the Equation (8), the Kissinger function curves of the samples could be acquired. It can be seen in Fig. 8 that the obtained data possessed good linearity, indicating that this equation was successful application for the as-prepared samples.

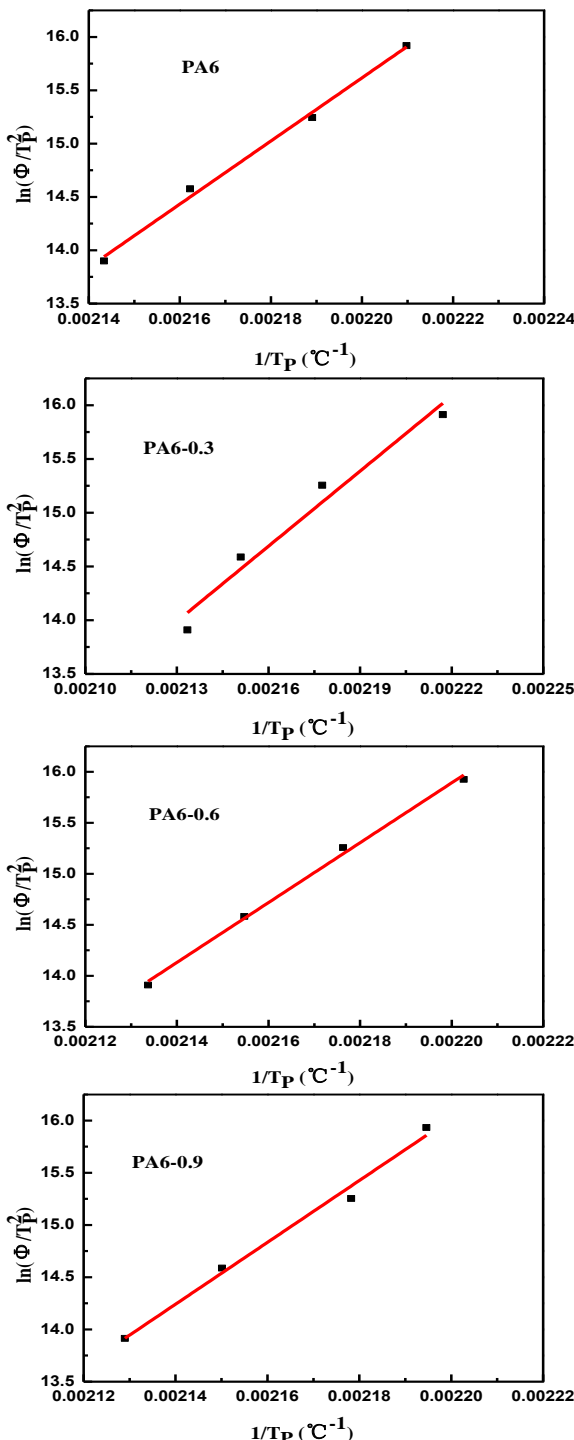


Fig. 8: The Kissinger function curves of the samples.

Generally,  $\Delta E$  can be contributed by the transport activation energy ( $\Delta E^*$ ) and the nucleation activation energy ( $\Delta F^*$ ). It is worth noting that the former is related to the movement of chain segments and the latter is in connection with the nucleation of the crystals. It can be acquired from the slope of the fitting straight-lines and  $R$ .

Table-4:  $\Delta E$  of the samples.

Samples	PA6	PA6-0.3	PA6-0.6	PA6-0.9
$\Delta E$ (kJ·mol <sup>-1</sup> )	-246.10	-193.53	-243.88	-246.10

In table 4, it can be found that the  $\Delta E$  was first decreased and then increased with increasing the GO-CNTs hybrids loading. It reached the minimum when the as-prepared hybrid loading was 0.3 wt%. The possible reasons could attribute to the follow two aspects. On the one hand, the GO-CNTs hybrids could hinder the movement of chain segments and then increase  $\Delta E^*$ . On the other hand, they could act as heterogeneous nucleis and then decrease  $\Delta F^*$ .

## Conclusion

In summary, the non-isothermal crystallization behaviors of GO-CNTs / PA6 composites were discussed by using the theories of Jeziorny, Ozawa, Mo and Kissinger, respectively. Based on the Jeziorny's theory, the overall  $G$  was increased with increasing  $\phi$  for pure PA6; however, it was first increased and then decreased for the as-prepared composites. Based on the Ozawa's theory, the overall  $G$  and the nucleation and growth modes showed a complicated variation driven by the crystallization temperature and  $\phi$ . Moreover, based on the Mo's theory, the  $G$  was first decreased and then increased with increasing the fillers loading. It reached a minimum value when the fillers loading were 0.6 wt%. In addition, based on the Kissinger's theory, the  $\Delta E$  was first decreased and then increased with increasing the fillers loading. When it was 0.3 wt%, the  $\Delta E$  was the minimum. These complicated results could be attributed to the hindering and promoting effects of the GO-CNTs hybrids coexisting during the crystallization process. These results can provide reference values for understanding the crystallization kinetics of the PA6 composites.

## Acknowledgements

Authors gratefully acknowledge the support from Natural Science Foundation of Hebei Province, China (Grant No. E2013210011). The authors declare that they have no conflict of interest.

## References

- Y. Liu and G. S. Yang. Non-isothermal crystallization kinetics of polyamide-6/graphite oxide nanocomposites. *Thermochim. Acta*, **500**, 13 (2010).
- X. F. Wu, Y. K. Zhao, H. Li, Z. H. Zhao, Y. Sun, H. Zhang, M.T. Yu and F. F. Jia. Non-isothermal crystallization kinetics of polyamide 6/h-boron nitride composites. *J. Macromol. Sci. B* **56**, 170 (2017).
- J. Baiju and F. Mutsuhisa. Enhanced mechanical properties of polyamide 6 fibers coated with a polyurethane thin film. *Polym. Eng. Sci.* **49**, 1970 (2009).
- X. F. Wu, Y. K. Zhao, X. J. Li, Y. J. Wang, C. X. Zhang, J. Z. Su, J. R. Zhang, K. Y. Wang, Y. W. Wang and M. Zhang. Isothermal crystallization properties of polyamide 6/hexagonal boron nitride Nanocomposites. *J. Macromol. Sci. B* **57**, 56 (2018).
- A. O'Neill, D. Bakirtzis and D. Dixon. Polyamide 6/Graphene composites: The effect of in situ polymerisation on the structure and properties of graphene oxide and reduced graphene oxide. *Eur. Pol. J.* **59**, 353 (2014).
- X. F. Wu, Z. H. Zhao, Y. Sun, H. Li, C. X. Zhang, Y. J. Wang, S. S. Zheng and H. Zhang. Few-layer boron nitride nanosheets: Preparation, characterization and application in epoxy resin. *Ceram. Int.*, **43**, 2274 (2017).
- G. M. Kim, G. H. Michler, F. Ania and F. J. Balta Calleja. Temperature dependence of polymorphism in electrospun nanofibres of PA6 and PA6/clay nanocomposite. *Polymer* **48**, 4814 (2007).
- J. S. Shi, X. J. Yang, X. Wang and L. D. Lu Non-isothermal crystallization kinetics of nylon 6/attapulgite nanocomposites. *Polym. Test.* **29**, 596 (2010).
- S. Şanlı, A. Durmus and N. Ercan. Isothermal crystallization kinetics of glass fiber and mineral-filled polyamide 6 composites. *J. Mater. Sci.* **47**, 3052 (2012).
- J. C. Liang, Y. Q. Xu, Z. Y. Wei, P. Song, G. Y. Chen and W. X. Zhang. Mechanical properties, crystallization and melting behaviors of carbon fiber-reinforced PA6 composites. *J. Therm. Anal. Calori.* **115**, 209 (2014).
- A. Yebra-Rodríguez, P. Alvarez-Lloret, C. Cardell and A. B. Rodríguez-Navarro. Crystalline properties of injection molded polyamide-6 and polyamide-6/montmorillonite nanocomposites. *Appl. Clay Sci.* **43**, 91 (2009).
- N. T. Dintcheva, R. Arrigo, G. Nasillo E. Caponetti and F. P. L. Mantia. On the role of extensional flow in morphology and property modifications of MWCNT/polyamide-based fibers. *Macromol. Mater. Eng.* **296**, 645 (2011).
- F. Zhang, X. C. Peng, W. B. Yan, Z. Y. Peng and Y. Q. Shen. Nonisothermal crystallization kinetics of in situ nylon 6/graphene composites by differential scanning calorimetry. *J. Polym. Sci. Pol. Phys.* **49**, 1381 (2011).
- F. Zhang, B. Wang, R. L. Man and Z. Y. Peng. Isothermal crystallization kinetics of in situ nylon 6/graphene composites by differential scanning calorimetry. *Polym. Eng. Sci.* **54**, 2610 (2014).
- H. Palza, B. Reznik, M. Wilhelm, O. Arias and A. Vargas. Electrical, thermal, and mechanical characterization of poly(propylene)/carbon nanotube/clay hybrid composite materials. *Macromol. Mater. Eng.* **297**, 474 (2012).
- C. Zhang, W. W. Tjiu, T. X. Liu, W. Y. Lui, I. Y. Phang and W. D. Zhang. Dramatically enhanced mechanical performance of nylon-6 magnetic composites with nanostructured hybrid one-dimensional carbon nanotube-two-dimensional clay nanoplatelet heterostructures. *J. Phys. Chem. B* **115**, 3392 (2011).
- H. M. Chen, L. N. Shao, Y. Shen, J. H. Yang, T. Huang, N. Zhang, Y. Wang and C. I. Zhang. Largely improved crystallization behavior and thermal stability of poly(L-lactide) via the synergistic effects of graphene oxide and carbon nanotubes. *J. Appl. Polym. Sci.* **131**, 631 (2014).
- Y. K. Kim, H. K. Na, S. J. Kwack, S. R. Ryoo, Y. Lee, S. Hong, S. Hong, Y. Jeong and D. H. Min. Synergistic effect of graphene oxide/MWCNT films in laser desorption/ionization mass spectrometry of small molecules and tissue imaging. *ACS Nano* **5**, 4550 (2011).
- Y. S. Hwang, M. J. Kim and J. H. Kim. Role of direct covalent bonding in enhanced heat dissipation property of flexible graphene oxide–carbon nanotube hybrid film. *Thin Solid Films* **545**, 116 (2013).
- H. Im and J. Kim. Thermal conductivity of a graphene oxide–carbon nanotube hybrid/epoxy composite. *Carbon* **50**, 5429 (2012).
- W. K. Li, A. Dichiara and J. B. Bai. Carbon nanotube-graphene nanoplatelet hybrids as high-performance multifunctional reinforcements in epoxy composites. *Compos. Sci. Technol.* **74**, 221 (2013).
- C. Zhang, S. Huang, W. W. Tjiu, W. Fana and T. X. Liu. Facile preparation of water-dispersible graphene sheets stabilized by acid-treated multi-walled carbon nanotubes and their

- poly(vinyl alcohol) composites. *J. Mater. Chem.* **22**, 2427 (2012).
- 23. J. Yan, T. Wei, Z. J. Fan and W. Z. Qian. Preparation of graphene nanosheet/carbon nanotube/polyaniline composite as electrode material for supercapacitors. *J. Power Sources* **195**, 3041 (2010).
  - 24. G. Q. Ning, T. Y. Li, J. Yan, C. G. Xu, T. Wei and Z. J. Fan. Three-dimensional hybrid materials of fish scale-like polyaniline nanosheet arrays on graphene oxide and carbon nanotube for high-performance ultracapacitors. *Carbon* **54**, 241 (2013).
  - 25. A. S. Patole, S. P. Patole, S. Y. Jung, J. B. Yoo, J. H. An and T. H. Kim. Self assembled graphene/carbon nanotube/polystyrene hybrid nanocomposite by in situ microemulsion polymerization. *Eur. Polym. J.* **48**, 252 (2012).
  - 26. X. F. Wu, Y. K. Zhao, Z. H. Zhao, Y. Sun, H. Zhang, M. T. Yu and F. F. Jia. Crystallization behaviors of graphene oxide-carbon nanotubes hybrids/polyamide 66 composites. *Polym.-Plast. Technol.* **56**, 556 (2017).
  - 27. A. Jeziorny. Parameters characterizing the kinetics of the non-isothermal crystallization of poly(ethylene terephthalate) determined by D.S.C. *Polymer* **19**, 1142 (1978).
  - 28. T. Ozawa. Kinetics of non-isothermal crystallization. *Polymer* **12**, 150 (1971).
  - 29. M. Y. Liu, Q. X. Zhao, Y. D. Wang, C. G. Zhang, Z. S. Mo and S. K. Cao. Melting behaviors, isothermal and non-isothermal crystallization kinetics of nylon 1212. *Polymer* **44**, 2537 (2003).
  - 30. H. E. Kissinger. Variation of peak temperature with heating rate in differential thermal analysis. *J. Res. Natl. Bur. Stand.* **57**, 217 (1956).